



Hydrogen production by glycerol steam reforming catalyzed by Ni-promoted Fe/Mg-bearing metallurgical wastes

Ommolbanin Ali Zadeh Sahraei^a, Faiçal Larachi^a, Nicolas Abatzoglou^b, Maria C. Iliuta^{a,*}

^a Department of Chemical Engineering, Université Laval, Québec, QC, G1V 0A6, Canada

^b Department of Chemical Engineering and Biotechnological Engineering, Université de Sherbrooke, Sherbrooke, QC, J1K 2R1, Canada



ARTICLE INFO

Article history:

Received 13 March 2017

Received in revised form 11 July 2017

Accepted 14 July 2017

Available online 17 July 2017

Keywords:

Industrial waste

Nickel catalyst

Solid-state impregnation

Glycerol steam reforming

Catalyst stability

ABSTRACT

The present work investigates the catalytic potential of a Ni-promoted Fe/Mg containing metallurgical waste for sustainable hydrogen production by glycerol steam reforming (GSR). The catalyst (Ni-UGS) was prepared through solid-state impregnation of Ni into the structure of metallurgical residue. Ni incorporation led to the formation of (Ni,Mg)O solid solution, (NiFe₂O₄) and/or a nickel iron mixed oxide (Ni_xFe_{1-x}O). GSR performed in a fixed bed reactor at T = 580 °C, P = 1 atm, steam to carbon ratio (S/C) of 3, and gas hourly space velocity (GHSV) of 20,600 cm³ (STP) g_{cat}⁻¹ h⁻¹ led to a glycerol conversion to gaseous (X_g) of 87%, H₂ yield (Y_{H2}) of 79%, and H₂/CO molar ratio of 5.5. The catalytic performance of Ni-UGS containing 11.7 wt.% Ni was found to be superior to that of an alumina supported Ni-based commercial steam reforming catalyst with higher Ni content (29.8 wt.%): X_g = 86%, Y_{H2} = 71%, and H₂/CO molar ratio of 4.1. A stable performance during 48 h on stream was also obtained by using the Ni-UGS catalyst. Characterization of the used catalyst confirmed the low formation rate (~2.7 mg_{coke} g_{cat}⁻¹ h⁻¹) of filamentous type carbon. The promising obtained results were mainly attributed to (i) superior dispersion of Ni particles due to the formation of (Ni,Mg)O solid solution and (ii) the presence of active magnesium and iron oxide species (e.g., MgO, Fe₂O₄, MgFe₂O₄ and (MgO)(FeO) solid solution) in the Ni-UGS catalyst which stimulate the water gas shift reaction and coke gasification. Regeneration by an oxidative treatment of the used catalyst in air was examined and analysis of the regenerated catalyst revealed complete coke removal together with recovery of initial crystalline phases.

© 2017 Elsevier B.V. All rights reserved.

1. Introduction

The increase of worldwide energy demand and environmental concerns are among the most challenging issues of the 21st century [1]. As an emissions-free alternative fuel, hydrogen has been receiving a growing interest as an option to alleviate the world energy crisis [2]. More than 95% of current hydrogen production is based on steam reforming of natural gas and other fossil resources [2]. However, either depletion of fossil fuel reserves or global warming caused by greenhouse gas emissions are questioning the use of fossil resource as feedstock for hydrogen production [3,4]. Recourse to using renewable feedstocks such as biomass or biomass-derived by-products can offer a sustainable and cost-competitive hydrogen production route. While hydrogen and syngas are generated from these renewable resources, biomass growth serves as a sink

for produced CO₂ thus offering a carbon dioxide neutral energy supply.

As an important by-product of biodiesel production, glycerol has emerged as a promising feedstock for green hydrogen generation [2]. Biodiesel has been already commercialized in several countries in the past two decades and its use is expected to grow due to its renewability and considerable reduction in CO₂ emissions compared to fossil fuels [5,6]. In common biodiesel synthesis through transesterification of triglycerides with methanol, around 0.1 ton of crude glycerol by-product is stoichiometrically produced per each ton of biodiesel [7]. By 2020, approximately 3 Mt of crude glycerol are expected to be produced, whereas the annual demand for commercial use is expected to be less than 0.5 Mt [8]. Considering the significant oversupply, there is a compelling need to valorize this by-product economically, thus avoiding it to become a waste problem and to adversely weigh on biodiesel industrial development [7–9]. Regarding the expected unlimited future market of hydrogen and the interest in switching to renewable sources for its production, hydrogen generation from glycerol is one of the promising alternatives [10].

* Corresponding author.

E-mail address: maria-cornelia.iluta@gch.ulaval.ca (M.C. Iliuta).

Various methods such as pyrolysis, steam reforming (SR), partial oxidation (PO), auto-thermal reforming (ATR), and aqueous-phase reforming (APR) have been proposed to valorize biodiesel by-product into hydrogen [11–14]. SR is amongst the most mature industrial technologies [12] and only few adjustments are required to shift from commonly used feedstocks to glycerol.

To enhance hydrogen production by glycerol steam reforming (GSR), the choice of appropriate catalysts is crucial. According to the literature, ruthenium (Ru), rhodium (Rh), platinum (Pt), nickel (Ni), and cobalt (Co) have shown catalytic activity in GSR [7]. Among them, catalysts with Ni supported on different inorganic oxides and their mixtures (such as Al_2O_3 , MgO , CeO_2 , ZrO_2 , TiO_2 , and SiO_2) [4,15,16] are the most investigated ones due to their low cost and high availability. However, while Ni is effective for the cleavage of $-\text{CH}_3$, $-\text{CH}_2-$, $\text{O}-\text{H}$, and $-\text{C}-\text{C}-$ bonds, its activity in water gas shift (WGS) reaction is limited beside its vulnerability to sintering and coke formation [17].

The surface properties of support materials used in the formulation of steam reforming catalysts can play an important role in enhancing WGS reaction and decreasing coke formation by oxidative removal of surface carbon deposits. One of the highly favored strategies is the utilization of oxides with good redox properties, such as rare-earth and transition-metal oxides (e.g., CeO_2) [18]. Promotion of the catalytic performance by enhancing water activation can also be achieved by using oxides with basic properties such as alkaline earth oxides (e.g., MgO) [19–21]. Moreover, the use of basic oxides has also been suggested for lowering the concentration of acidic sites on the surface of acidic supports such as Al_2O_3 . Dehydration of alcohols leads to alkenes production in the presence of strongly acidic surface sites leading to carbon deposition [19–21]. In addition, improved dispersion of Ni particles together with stronger interactions with the support through mediation of promoters, e.g., Mg, Ce and La, can also prevent coke formation [22].

New types of catalysts have also been developed by dispersing active metal phase on metal oxide matrix precursors such as perovskites (e.g., $\text{LaNi}_x\text{Fe}_{(1-x)}\text{O}_3$ and $\text{La}_{1-x}\text{Ce}_x\text{NiO}_3$) [23,24], Mg-Al hydrotalcite [25,26], and mixed oxide spinels (e.g., NiAl_2O_4 and NiFe_2O_4) [27–30]. Mineral-type precursors [31,32] (like olivine [33,34]), with homogeneously distributed exchangeable metal cations in the crystal structure, are the other proposed materials to obtain a good dispersion of Ni particles and to benefit from the presence of elements, such as Mg and Fe, inside these materials. It has been reported that in some of these structures, highly dispersed metal particles formed in a reducing atmosphere exhibited high activity and stability in reforming reactions [30]. Moreover, the reduction of such catalysts may sometimes result in the combination of Ni with another element of the structure, to form a bimetallic species or alloy with improved catalytic performance [35]. In the case of Ni-olivine catalysts used in steam reforming reactions, it was suggested that the formation of various Ni-Fe alloys [36,37] and $(\text{Ni},\text{Mg})\text{O}$ solid solutions [34,38] limited coke formation.

Currently, about 65 kt of solid oxide residues are yearly produced in a production process of upgraded titania-rich slag (UGS) from hemo-ilmenite ore ($\text{FeTiO}_3\text{-Fe}_2\text{O}_3$), at Rio Tinto Iron & Titanium (RTIT) Company located in the metallurgical complex of RTIT in Sorel-Tracy (Québec, Canada). Without marketable use, this residue (UGS oxides) is disposed of in a mining waste site (P- 84, Sorel-Tracy). The elements composing this residue are mainly Fe, Mg and Al aggregating in the form of crystalized spinel groups of magnesioferrite (MgFe_2O_4), hercynite (FeAl_2O_4) and free periclase (MgO) [39]. Considering the magnesium and iron oxide species present in the residue, with several reported promoting effects in the formulation of steam reforming catalysts [19–22,25,33,34,38,40,41], this solid waste can be explored as an appropriate precursor for incorporating more active metals inside its spinel structure. This has been demonstrated in our recent study

on nickel-borne UGS oxides which proved very efficient for the catalytic dry reforming of methane [42].

Solid state impregnation (SSI) is a facile, energy efficient and time saving method for preparation of mixed oxides for different applications including catalysis [43–46]. This method involves grinding of the reactants and subsequent calcination of the precursors to decompose them into corresponding oxides and does not require drying, purification or recycling of solvents [43]. Small amounts of volatile liquids (e.g., acetone, alcohol) can only be used as mixing homogenizers (they usually volatilize completely after less than 10–15 min of grinding) [47]. In comparison with conventional wet impregnation method, higher dispersion of active metal species, stronger metal-support interactions and enhanced catalytic performance were reported by several authors for the catalyst synthesized by SSI [43].

The aim of this study is to investigate the potential of Ni incorporated UGS oxides residue (Ni-UGS) as catalyst in glycerol steam reforming for hydrogen production. Ni was incorporated in the UGS oxides residue by SSI and the synthesised catalysts were characterized by XRD, ICP, TEM, and BET. Hydrogen yield, glycerol conversion, stability and regenerability of Ni-UGS catalyst were evaluated.

2. Materials and methods

2.1. Catalyst preparation

The as-received fine agglomerates of UGS oxides residue (hereinafter called as UGS) was ground to fine powder and sieved to particle size less than 75 μm prior to use. The Ni-UGS catalyst was prepared based on the SSI method described above [43–47], by incorporating 12.5 wt.% Ni into the UGS residual material. For this purpose, nickel nitrate hexahydrate $\text{Ni}(\text{NO}_3)_2\cdot6\text{H}_2\text{O}$ (Fisher, 99.9%) precursor and UGS were weighed out in their required amounts and then ground in an agate mortar at ambient temperature for about 20 min. Acetone used to help homogenization was gradually evaporated during mixing after ca. 10 min. The sample was calcined under air flow (200 mL min^{-1}) at 600 $^\circ\text{C}$ for 5 h. Finally, the resulting solid was ground and sized afresh to particle sizes less than 75 μm before characterisation and use in the reforming tests.

2.2. Material characterization

Elemental analyses were carried out by inductively coupled plasma mass spectrometry (ICP-MS) using a Perkin-Elmer Optima 3300DV apparatus. Crystalline phases were characterized by X-ray diffraction (XRD) on a Siemens D5000 X-ray powder diffractometer using a $\text{Cu K}\alpha$ radiation (wavelength $\lambda = 1.54059 \text{\AA}$) generated at 40 kV and 30 mA. The diffraction angles, 2Θ , ranged from 10 $^\circ$ to 80 $^\circ$ with a sweep of 1 $^\circ/\text{min}$. The particle size and morphology of catalyst as well as the type of coke formed on the reacted catalyst were examined by transmission electron microscopy (TEM) on a JEOL JEM 1230 electron microscope with an accelerating voltage of 80 kV. The samples were dispersed in anhydrous ethanol using an ultrasonic bath and then a drop of produced suspension was placed onto a copper grid coated with carbon films and dried at room temperature naturally. Nitrogen adsorption-desorption isotherms (BET) were obtained with a Quantachrome Autosorb-1 system. BET surface areas were determined in the range of 0.05–0.3 P/P0. Before measurements, the samples were outgassed under vacuum for 6 h at 150 $^\circ\text{C}$. Thermogravimetric analysis (TGA) (Perkin Elmer Lab System Diamond TGA-DTA) coupled with mass spectrometry (MS) with quadrupole analyzer (Thermostar Prisma QMS200, Pfeiffer Vacuum) was used to study the solid state reaction of Ni precursor and UGS, and investigate the carbon deposited on catalyst. The

samples were loaded in alumina crucibles and heated at a rate of 10 °C/min under air flow (50 mL min⁻¹) from room temperature to 1000 °C (800 °C for coke analysis). Changes in sample mass as well as the evolved gases were monitored as a function of time.

2.3. Evaluation of catalyst activity

To evaluate the performance of prepared catalyst for H₂ production by GSR, the reaction was performed in a stainless steel tubular fixed-bed reactor (11 mm internal diameter and 40 cm length) under atmospheric pressure. 0.5 g of catalyst sample was loaded on a grid support fixed in the middle of the reactor and covered with quartz wool. Temperature was controlled by a thermo-controller (Omega, CN-7800) connected to a k-type thermocouple located inside the catalytic bed. Before introducing any reactant, the reactor was purged with argon for 30 min. Prior to GSR reaction, an in-situ reduction pre-treatment at 650 °C for 1.5 h by a mixture stream of H₂/argon (total flow of 50 STD mL min⁻¹ with 20 vol% H₂) was performed to activate the catalyst. The reactor was then cooled down to the reaction temperature of 580 °C in a stream of pure argon to purge residual hydrogen. Hydrogen and argon flows were controlled using Omega (FMA-2620A) mass flow meters.

After reaching the reaction temperature, a feed mixture of pure glycerol (Caledon, ≥99.5%) and water with a water/glycerol molar ratio of 9 (steam to carbon molar ratio (S/C) of 3) was injected into the pre-heater by a gas-tight glass syringe mounted in a New Era syringe infusion pump (NE-1000). The preheating section consisted of a horizontal spiral coil located inside a furnace and its temperature was controlled by a thermo-controller (Omega, CN-7800) connected to a k-type thermocouple located outside the spiral coil. The reactant mixture of glycerol and water were vaporized in the preheater and then mixed with argon as a carrier gas prior the feeding into the reforming reactor. The temperature of pre-heater and the line connecting the preheating section to the reactor were maintained at 300–350 °C. The flow rate of argon was set to obtain a molar ratio of feeding reactant (glycerol + water mixture) to inert gas (argon) F.I of 1:4. The gas hourly space velocity (GHSV) at the standard temperature and pressure (STP) was calculated to be 20,600 cm³ g_{cat}⁻¹ h⁻¹. The reactor outlet stream entered the condenser to separate condensable products. The gaseous reaction products were then analyzed on-line by microGC (Agilent Technologies, 3000A).

Glycerol conversion to gaseous products (X_g) was calculated on the basis of the carbon balance (Eq. (1)):

$$X_g (\%) = \frac{\text{moles of C atoms in the gaseous products}}{3 \times \text{moles of glycerol in the feed}} \times 100 \quad (1)$$

Hydrogen yield (Y_{H2}) was calculated based on the maximum stoichiometric ratio of 7 between hydrogen and glycerol (Eq. (2)):

$$Y_{H_2} (\%) = \frac{\text{moles of } H_2 \text{ produced}}{7 \times \text{moles of glycerol in the feed}} \times 100 \quad (2)$$

To perform carbon balance, the carbon content of the condensable by-products was measured by CHNS analysis (EA 1108, Fisons, CHNS). Moreover, the amount of deposited carbon was determined by burning it *in-situ* with air after each experiment and measuring the amount of CO₂ evolved by microGC. A carbon balance error (defined as |1 - m_{outlet carbon}/m_{inlet carbon}|) less than 5% was calculated for all glycerol steam-reforming tests presented in this study.

Thermodynamic equilibrium concentrations were calculated by Aspen Plus V9 software based on direct minimization of Gibbs free energy and used to estimate glycerol conversion, H₂ yield and product distribution. The experimental data were compared to the theoretical values to investigate if equilibrium was reached.

Table 1
Chemical composition (wt.%) of UGS oxides residue.

Analyte	Fe	Mg	Al	Ca	Mn	V	Ti
UGS oxides residue	31.26	17.49	5.35	1.05	0.98	0.92	0.61

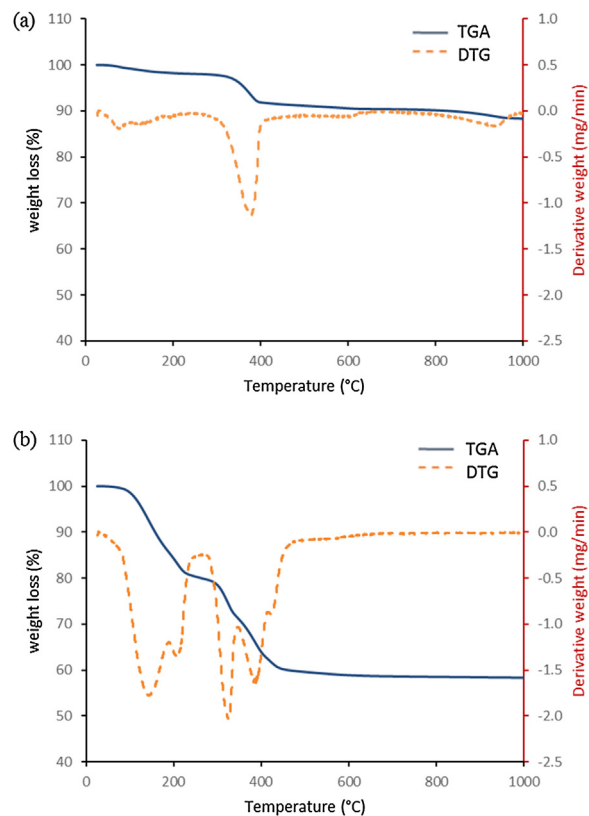


Fig. 1. TG/DTG curves for (a) as-received UGS oxides residue (b) as-prepared Ni-UGS (before calcination step).

3. Results and discussion

3.1. Characterization of UGS oxides residue and Ni-UGS catalyst

Elemental analysis of as-received UGS oxides residue using ICP-MS (**Table 1**) revealed that iron (32 wt.%), magnesium (18 wt.%), and aluminium (5 wt.%) are the main constitutive elements of the material and other elements such as Ca, Mn, Ti, and V are present in much lesser extent.

Fig. 1 shows the TGA results and the corresponding differential thermogravimetric (DTG) curves of UGS without any modification (as-received UGS) and Ni incorporated UGS before air-calcination (as-prepared Ni-UGS) in the range of ambient temperature to 1000 °C. According to **Fig. 1a**, the as-received UGS showed about 12% total weight loss that occurred in the ranges of 25–200 °C and 280–430 °C. The first region can be assigned to the loss of physisorbed water, while the second to the dehydroxylation of magnesium hydroxide (Mg(OH)₂) into periclase (MgO) [48]. The two other minor weight losses (totally about 3%) in TG curve of as-received UGS, which occurred in the ranges of 430–600 °C and 820–980 °C, can be attributed to crystal-phase changes of the material. According to **Fig. 1b**, a total weight loss of about 42% was observed during the decomposition of Ni-UGS up to 1000 °C, with two main intervals accompanied by five peaks of weight loss rate in the DTG curve. The first interval (25–240 °C) with two DTG minima at about 146 °C and 215 °C can be assigned to the loss of adsorbed water and crystal water of initial nickel nitrate

Table 2
BET surface area.

Sample	BET surface area ($\text{m}^2 \text{ g}^{-1}$)
As received-UGS	8.5
Fresh Ni-UGS	10.3
Used Ni-UGS ^a	59.5
Regenerated Ni-UGS	7.9

^a after 48 h on GSR reaction.

hexahydrate reagent [49,50]. The weight losses in the second temperature region (285–480 °C), with three DTG minima at about 326 °C, 390 °C, and 425 °C, can be attributed to the decomposition of nickel nitrate [51,52], dehydroxylation of magnesium hydroxide (Mg(OH)_2) [48] and formation of new crystal phases. As can be seen from TG curve of Ni-UGS (Fig. 1b), there is almost no loss of weight after 600 °C, suggesting that the nickel precursor decomposed completely up to this temperature with new phases formed, which has been further investigated by XRD. It was therefore concluded that 600 °C could be a suitable calcination temperature for the Ni-UGS catalyst.

Fig. 2 compares the X-ray diffractograms of as-received UGS and Ni-UGS. According to Fig. 2a, the major mineral phases of UGS oxides residue are spinel groups of magnesioferrite (MgFe_2O_4) and hercynite (FeAl_2O_4), which mutually co-exist in a $\text{Mg}(\text{Al}_x \text{Fe}_{2-x})\text{O}_4$ solid solution [39]. Magnetite(Fe_3O_4) (ICDD file No. 01-075-0449) and brucite (Mg(OH)_2) (ICDD file No. 01-074-2220) were also detected. After Ni incorporation into UGS structure by SSI method (Fig. 2b), the diffraction lines of Mg(OH)_2 at $2\Theta = 18.594^\circ, 37.998^\circ, 50.845^\circ$, and 58.621° (ICDD file No. 01-074-2220) disappeared as a result of thermal treatment (calcination of material at 600 °C for 5 h under air flow). Moreover, the appearance of new line at $2\Theta = 37.1^\circ$ and intensification of peaks with maximum at $2\Theta = 43.1^\circ, 62.9^\circ, 74.7^\circ$, and 79.08° were also observed, which can be assigned to the formation of NiO ($2\Theta = 37.23^\circ, 43.26^\circ, 62.84^\circ, 75.37^\circ$ and 79.36°) (ICDD file No. 01-078-0423), MgO ($2\Theta = 37.13^\circ, 43.14^\circ, 62.66^\circ, 75.14^\circ$ and 79.11°) (ICDD file No. 01-075-1525) and/or a solid solution between these oxides as $(\text{Mg},\text{Ni})\text{O}$ ($2\Theta = 37.11^\circ, 43.10^\circ, 62.60^\circ, 75.09^\circ$ and 79.06°) (ICDD file No. 00-024-0712). Since MgO is a good solvent for the 3d-block transition metal ions, such as Ni^{+2} and Co^{+2} [53], it can be concluded that the formation of $(\text{Mg},\text{Ni})\text{O}$ solid solution is more likely to occur. The formation of this solid solution can result in a better dispersion of Ni^{+2} . Furthermore, the intensity of peaks at $2\Theta = 30.3^\circ, 35.7^\circ, 53.74^\circ$ and 57.4° was also amplified, possibly due to the formation of NiFe_2O_4 ($2\Theta = 30.27^\circ, 35.74^\circ, 37.28^\circ, 43.47^\circ, 53.88^\circ, 57.55^\circ$ and 62.72°) (ICDD file No. 00-003-0875) and/or a nickel iron mixed oxide ($\text{Ni}_x\text{Fe}_{1-x}\text{O}$) such as $\text{Ni}_{1.43}\text{Fe}_{1.7}\text{O}_4$ ($2\Theta = 30.26^\circ, 35.64^\circ, 37.29^\circ, 43.32^\circ, 57.31^\circ$ and 62.94°) (ICDD file No. 01-080-0072). It should be noted that a precise identification of new formed phases after Ni incorporation in UGS structure is not possible due to the overlapping of the most intense XRD peaks corresponding to the probable phases formed in the system.

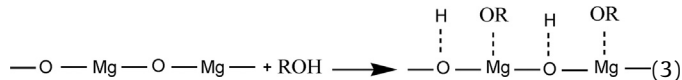
The final nickel loading of Ni-UGS catalyst, determined by ICP-MS analysis, was found to be 11.7 wt.%. As reported in Table 2, the BET surface area of UGS oxides residue and Ni-UGS are $8.5 \text{ m}^2 \text{ g}^{-1}$ and $10.3 \text{ m}^2 \text{ g}^{-1}$, respectively.

3.2. Catalytic performances in glycerol steam reforming

The catalytic performance and gas products distribution of glycerol steam reforming over Ni-UGS catalyst was investigated in a continuous fixed-bed reactor. All GSR tests were conducted at $T = 580^\circ\text{C}$, $P = 1 \text{ bar}$, water to glycerol feed molar ratio (WGFR) of 9:1 ($S/C = 3$) and feeding reactant (glycerol + water) to inert gas (Ar) molar ratio (FI) of 0.25, considered as optimum conditions according to a detailed thermodynamic analysis [54].

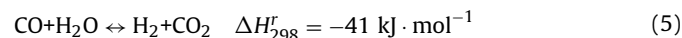
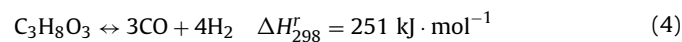
First, a blank (catalyst-free) experiment was carried out to determine the amount of hydrogen that could be produced as a result of glycerol thermal decomposition and its reaction with water. Second, the activity of the as-received UGS without any treatment was examined to study its ability to catalyze GSR. Finally, the performance of the prepared Ni-UGS catalyst was compared with that of a commercial alumina-supported nickel steam reforming catalyst (Hifuel™, Johnson Matthey Catalysts (UK) with 29.8 wt.% Ni content and BET surface area of $24.99 \text{ m}^2 \text{ g}^{-1}$). All tests were performed at the same operating conditions mentioned above.

Fig. 3a–c, presents the averages of glycerol conversion, hydrogen yield, gas product distribution, and H_2/CO molar ratio for the above-mentioned experiments carried out for a run time of 4 h. During this period, no significant catalyst deactivation was observed and the product distribution was approximately constant. The experimental results were compared with those at thermodynamic equilibrium at the mentioned operating condition. The weight of total deposited carbon on Ni-UGS and commercial catalyst at the end of 4 h GSR test, was measured by TGA analysis and reported as the percentages of total inlet carbon. The results are showed in Fig. 3d. As can be seen, in the selected reaction conditions, both glycerol conversion to gaseous products and hydrogen yield in the blank test were quite low ($X_g = 7\%$ and $Y_{\text{H}_2} = 4\%$, respectively). The catalytic performance of as-received UGS was better as compared to the blank reaction ($X_g = 23\%$ and $Y_{\text{H}_2} = 14\%$), but still of modest appeal to claim status for an efficient catalyst. Although metallic iron is known to have catalytic activity in steam reforming processes, it is less effective than other active metals such as Ni [41]. For example, Toshihide et al. [55] compared the catalytic activity of several catalysts supported on La_2O_3 for GSR and reported the following order: $\text{Ru} \simeq \text{Rh} > \text{Ni} > \text{Ir} > \text{Co} > \text{Pt} > \text{Pd} > \text{Fe}$. It has also been stated that the presence of ion pairs on the surface of alkaline earth metal oxides (especially MgO) can heterolytically cleave alcohols to give RO^- and H^+ (Eq. (3)) [53]. Therefore, the better performance of as-received UGS in comparison with the blank test may also be attributed to the dehydrogenation of glycerol by the MgO existing in the as-received UGS.



The average glycerol conversion, hydrogen yield, and H_2/CO molar ratio over Ni-UGS are $X_g = 87\%$, $Y_{\text{H}_2} = 79\%$, and 5.5, respectively. As can be seen in Fig. 3b, the gaseous concentrations in experimental results of Ni-UGS catalyst are near those predicted by thermodynamic equilibrium calculations. At same operating conditions, $X_g = 86\%$, $Y_{\text{H}_2} = 71\%$, and H_2/CO ratio of 4.1 were obtained for the commercial Ni-based steam reforming catalyst.

Generally, glycerol steam reforming (GSR) mainly involves pyrolysis of glycerol to produce syngas (Eq. (4)) whereas H_2 production is further promoted by water gas shift reaction in the presence of steam (Eq. (5)) [11]. Consequently, the overall reaction of GSR is represented by Eq. (6) [7].



The product distribution in GSR is strongly affected by catalyst formulation. The higher activity of catalyst in water gas shift reaction will help removing the adsorbed CO from the catalyst surface and increase H_2 production. It is worth mentioning that the Ni-UGS catalyst achieved higher hydrogen yield and H_2/CO ratio despite its lower Ni content (11.7 wt.%) in comparison with the commercial catalyst (29.8 wt.%). Moreover, as can be seen in Fig. 3d, the amount

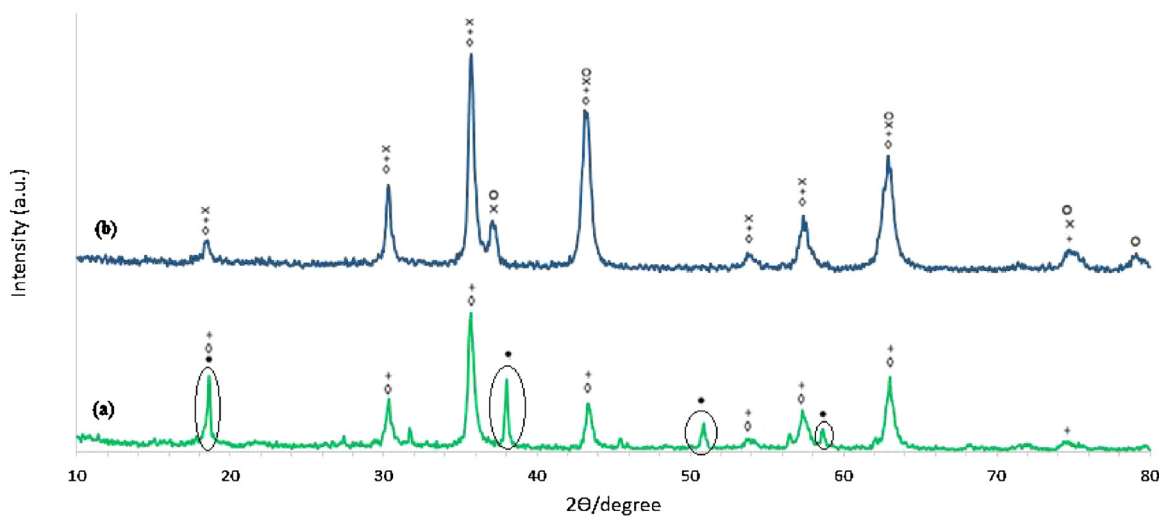


Fig. 2. X-ray powder diffraction patterns of (a) as-received UGS oxides residue (b) Ni-UGS. Crystalline phases: (\diamond) $Mg(Al_x Fe_{2-x})O_4$, (+) Fe_3O_4 and $MgFe_2O_4$, (●) $Mg(OH)_2$, (\bigcirc) $(Ni,Mg)O$, (\times) $NiFe_2O_4$.

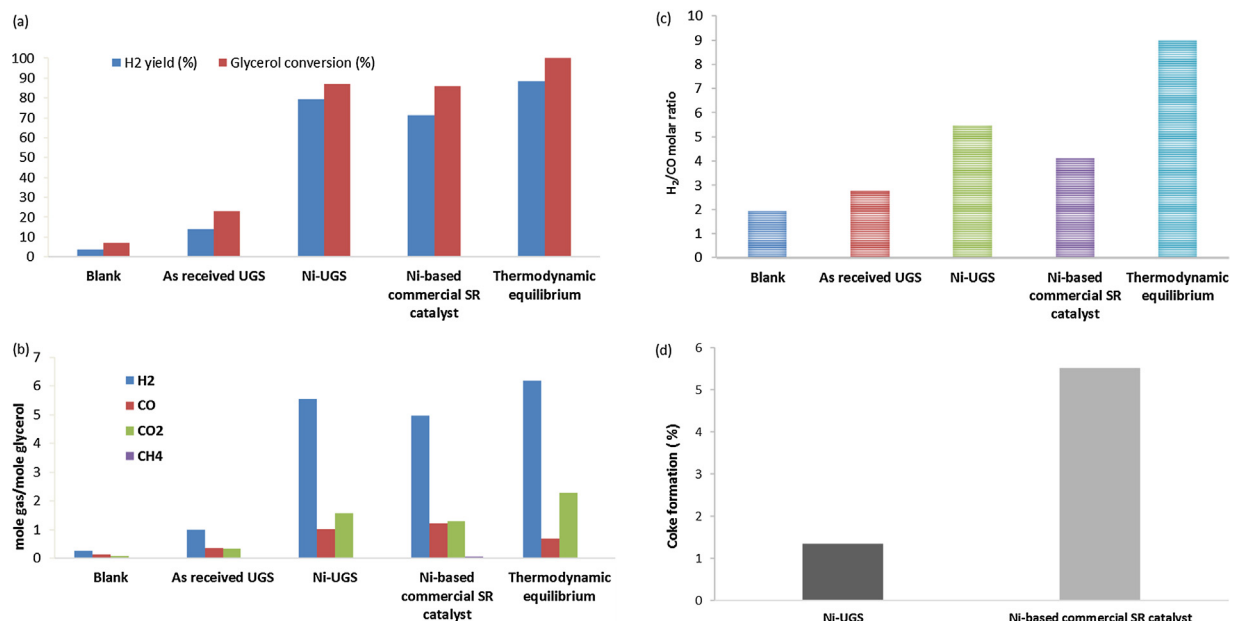


Fig. 3. Catalytic performances in GSR reaction: (a) glycerol conversion to gaseous products and hydrogen yield; (b) gas products distribution; (c) H₂/CO molar ratio; (d) Coke formation. Reaction conditions: T = 580 °C; P = 1 atm; S/C = 3; FI = 0.25; GHSV = 20,600 cm³ (STP) g_{cat}⁻¹ h⁻¹ and time on stream (TOS) = 4 h.

of coke formation is significantly lower in case of Ni-UGS catalyst. In comparison with the alumina support of the Ni-based commercial catalyst used in this study, these results confirm the superiority of UGS oxides metallurgical waste in promoting the water gas shift reaction and the lower tendency to form carbonaceous deposits. The results will be discussed more in details in §3.4.

3.3. Ni-UGS catalyst stability

To assess stability of Ni-UGS, its catalytic performance was investigated during 48 h on stream. According to Fig. 4, time-indifferent results were obtained for glycerol conversion to gaseous products, hydrogen yield and gas product distribution. Generally, sintering and coke formation are the two main causes for catalyst deactivation in steam reforming processes. A relatively lower reforming temperature is required when oxygenates (e.g., glycerol and ethanol) are used as feedstocks instead of hydrocarbons which

tends to delay sintering of metal particles. However, coke formation on the metal surface was found to occur in a much higher extent and it mostly deactivates the catalysts in the first hours on stream [18]. These results will be discussed in §3.5 where the phenomenon of coke formation on used Ni-UGS catalyst is examined.

3.4. Structural changes in reduced and used Ni-UGS catalyst

To make sense of the nature of active centers of Ni-UGS and catalyst stability during GSR reaction, the changes in the crystal structure of catalyst after the mentioned pre-reduction step (reduced catalyst) and after 48 h GSR reaction (used catalyst) were investigated by XRD (Fig. 5). Comparing the XRD patterns of fresh Ni-UGS (Fig. 5a) and reduced catalyst (Fig. 5b) shows that the intensity of the main peak at $2\Theta = 35.7^\circ$ decreased as a result of reduction pre-treatment. This peak is the main line for $NiFe_2O_4$ (and/or a nickel iron mixed oxide ($Ni_xFe_{1-x}O$)), magnesium alu-

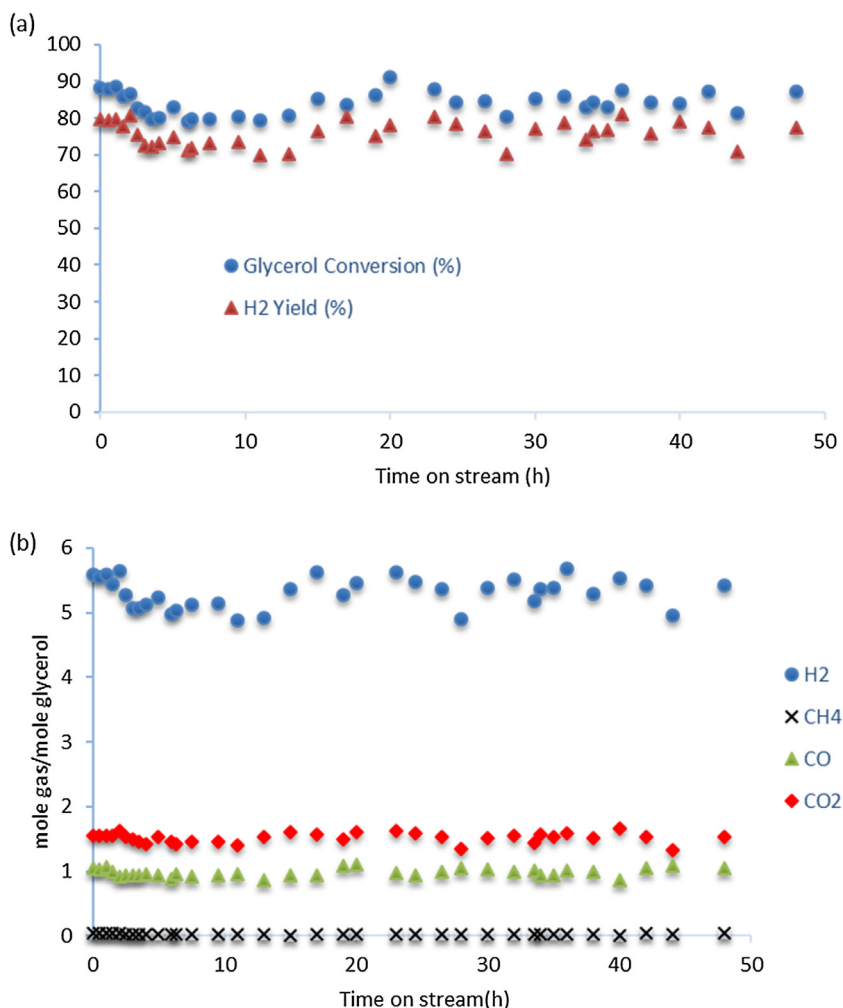


Fig. 4. Catalytic performance of Ni-UGS in GSR: (a) glycerol conversion to gaseous products (%) and hydrogen yield (%); (b) gas products distribution. Reaction conditions: T = 580 °C; P = 1 atm; S/C = 3; Fl = 0.25; GHSV = 20,600 cm³ (STP) g_{cat}⁻¹ h⁻¹ and time on stream (TOS) = 48 h.

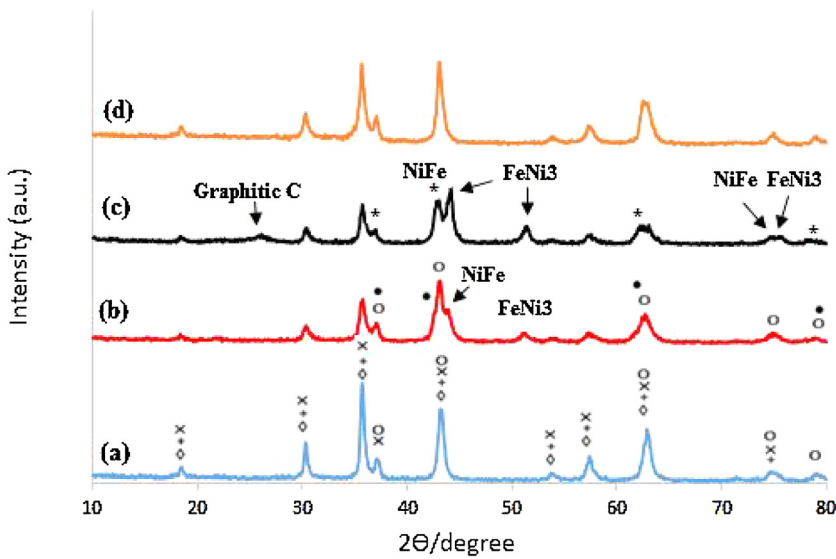


Fig. 5. X-ray powder diffraction patterns for (a) fresh, (b) reduced, (c) used, and (d) regenerated, Ni-UGS catalyst. Crystalline phases: (\diamond)Mg(Al_x Fe_{2-x})O₄, (+)MgFe₂O₄, (\circ)(Ni,Mg)O, (\times)NiFe₂O₄, (*)MgO, (\bullet)(MgO)_{1-x}(FeO)_x.

minum iron oxide (Mg(Al_x Fe_{2-x})O₄), and magnetite (Fe₃O₄) phases. Moreover, new peaks at $2\Theta = 43.92^\circ$ and 51.24° appeared, which are attributed to the formation of Ni-Fe alloys (such as NiFe, FeNi₃)

(ICDD file No. 00-012-0736 and ICDD file No. 00-038-0419). Furthermore, the diffraction lines related to (MgO)_{1-x}(FeO)_x solid solution ($2\Theta = 36.81^\circ$, 42.77° , 62.08° , 74.41° , 78.33° ICDD file No.

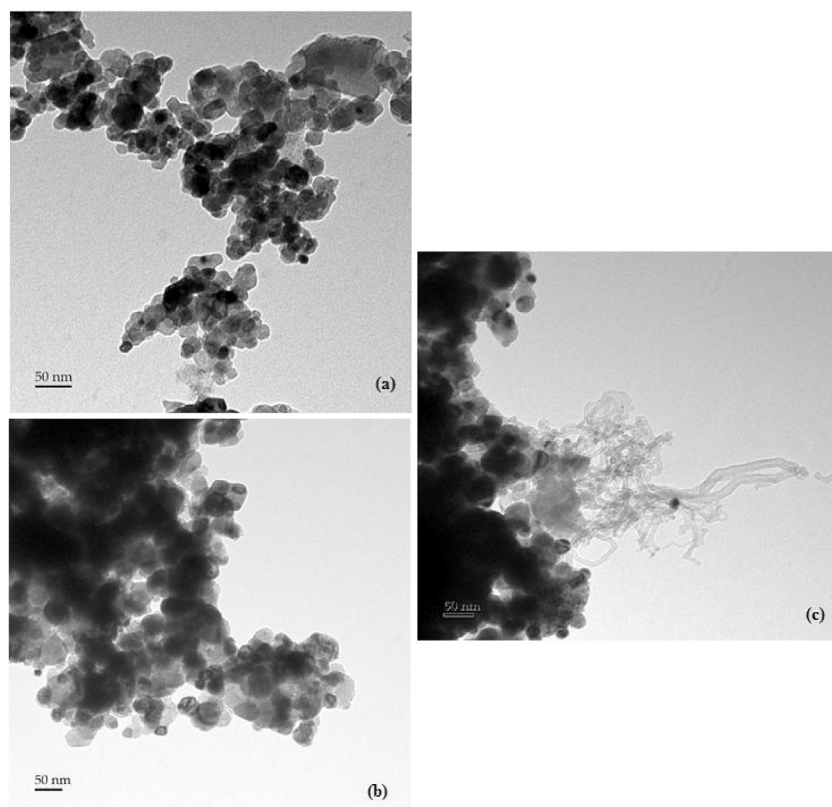
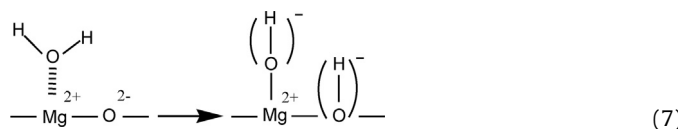


Fig. 6. Transmission electron micrographs (TEM) of Ni-UGS catalyst: (a) fresh, (b) used (after 48 h on GSR) and (c) coke formed on used catalyst.

01-077-2365) were also detected in the reduced sample. It should be noted that $(\text{Ni},\text{Mg})\text{O}$ solid solution ($2\Theta = 37.12^\circ, 43.14^\circ, 62.63^\circ, 75.09^\circ, 79.09^\circ$) (ICDD file No.00-034-0410) is the predominant phase in the reduced Ni-UGS sample. According to XRD analyses, the obtained GSR results can be partly attributed to good dispersion of Ni particles owing to the presence of $(\text{Ni},\text{Mg})\text{O}$ solid solution in the reduced catalyst. Moreover, as discussed in §3.2 (Eq. (3)), the presence of MgO can also help dehydrogenation of glycerol.

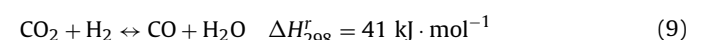
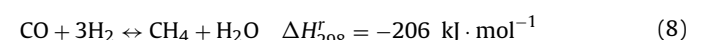
Another feature of Ni-UGS is the presence of different magnesium and iron oxide species (such as $(\text{Ni},\text{Mg})\text{O}$, MgFe_2O_4 , $(\text{MgO})(\text{FeO})$ solid solution, and Fe_3O_4) in the crystal structure of the reduced catalyst, which can help water activation and promote water gas shift reaction. Generally, the metal surface is the principal active site for dehydrogenation or C–C and C–O bonds dissociation of oxygenates in steam reforming process. As a result, surface-bound protons, carbonyl groups, carbon and oxygen species can be formed on the surface of catalyst. Oxidation of the adsorbed surface carbon species by water, as steam-reforming oxidant, plays an important role in the selectivity and stability of catalyst [18]. Since activation of water on metal sites is relatively difficult, one of the approaches is the use of oxides with good basic and redox properties, which can help water activation and promote water gas shift reaction [18]. Magnesium oxide is known for its ability in heterolytic cleavage of water (Eq. (7)) [53]:



An associative mechanism for MgO and MgFe_2O_4 as WGS catalysts has been reported by Rethwisch and Dumesic [56]. Magnetite-based catalysts are also well-known for high-temperature WGS reaction, based on regenerative mechanism [56]. However, it has

been reported that the use of alkaline or alkaline-earth metals as promoters with basic characteristics promotes associative mechanism in magnetite-based WGS catalysis. Boudjemaa et al. [57] reported high activity for hematite- (later in reaction, magnetite) supported MgO catalyst in high temperature shift reaction. By using in-situ DRIFT measurements, an associative mechanism was confirmed with formate intermediates produced by reaction of the hydroxyl groups on the Fe– MgO interface with the carbonyl species adsorbed on Fe.

As can be seen in Fig. 5b, part of the Ni-UGS catalyst was reduced to Ni-Fe alloys after the pre-reduction step. Several authors reported a promoting effect of Fe in Ni-based steam reforming catalysts when Ni-Fe alloys are formed after reduction or during steam reforming reaction [25,40,41]. Ashoke et al. [40] reported that Fe species in Ni-Fe alloys presented in the reduced $\text{Ni}/\text{Fe}_2\text{O}_3-\text{Al}_2\text{O}_3$ catalyst are partially oxidized to form intermediary FeO species endowed with good redox property. The redox behavior of Fe species enables them to switch easily between their oxidation states and increase the surface coverage of oxygen containing species. They enhance the steam reforming reaction and suppress coke formation. The main drawback of Ni-Fe alloys is the hydrogenating power of iron which favors the side reactions such as methanation (Eq. (8)) and reversed water gas shift (RWGS) (Eq. (9)) [58–60], resulting in low activity and low H_2/CO ratio.



However, Watanabe et al. [61] showed that FeNi_3 highly dispersed over a reducible oxide support (mesoporous $\text{CeO}_2-\text{ZrO}_2$) with a good transfer rate of lattice oxygen, can effectively suppress methanation side reaction at high temperature WGS reaction. The high H_2/CO ratio and low concentration of CH_4 obtained with Ni-

Table 3
Average particles size.

Sample	Average particles size (nm)
Fresh Ni-UGS	23 ± 6
Used Ni-UGS ^a	36 ± 10

^a after 48 h on GSR reaction.

UGS catalyst (Fig. 3b and c) show that the contribution of WGS reaction overcomes methanation and RWGS reactions.

Slight structural changes occurred for Ni-UGS catalyst during 48 h on reaction. As can be seen in the XRD pattern of used catalyst (Fig. 5c), the reflections assigned to (Ni,Mg)O solid solution at $2\Theta = 43.14^\circ$ and 62.7 became less pronounced. Moreover, the intensity of the lines related to Ni-Fe alloys at $2\Theta = 44.14^\circ$ and 51.42° was amplified and new lines related to MgO phase at $2\Theta = 43.04^\circ$ and 62.52° have appeared. A reflection line attributed to coke with graphite-like structure at $2\Theta = 26.1^\circ$ was also detected (ICDD file No. 00-003-0401).

TEM images (Fig. 6) and Digimizer image analysis software were used to evaluate the changes in morphology and size of Ni-UGS particles (Table 3) after 48 h on GSR. As can be seen in Fig. 6 (a, b) and Table 3, the used Ni-UGS catalyst shows the same morphology as fresh Ni-UGS with a slight averaged size increase from around 23 nm to 36 nm, indicating the slow tendency of catalyst particle to sintering.

3.5. Coke formation on used Ni-UGS catalyst

Carbon deposition, which is the main cause for catalyst deactivation in GSR process, was studied by TEM, TGA and BET analyzes of used Ni-UGS catalyst (after 48 h on reaction). Fig. 6c shows the presence of tubular filaments of carbon with metallic nickel on the tip of the fibers in the TEM micrograph of used Ni-UGS. The presence of graphitic carbon is in agreement with XRD analysis (Fig. 5c). As can be seen in Table 2, formation of filamentous type carbon with high surface area caused an increase in the BET surface area of the used Ni-UGS ($59.5 \text{ m}^2 \text{ g}^{-1}$) in comparison with that of fresh catalyst ($10.3 \text{ m}^2 \text{ g}^{-1}$). The BET surface area practically retrieved its initial value (Table 2) after regeneration (§ 3.6), which led to carbon removal.

Fig. 7 and Table 4 show the results of TGA-MS analysis of used Ni-UGS catalyst. The weight loss of 0.6 wt.% observed in the range of 25–200 °C can be attributed to water removal. The TGA profile (Fig. 7) outreaches the 100% and shows a mass gains of 2.6% in the range of 200–440 °C due to the oxidation of reduced species (e.g., metallic nickel and iron or their alloys) formed during the reforming reaction. The CO₂ evolved from the sample was detected by mass spectroscopy in the range of 440–600 °C (Fig. 7), which is a result of the oxidation of carbonaceous deposits. Since the oxidation of reduced species interfered with coke burning during TGA in air (in the range of 440–600 °C), an accurate quantification of the coke content is not possible based on Fig. 7. To estimate the rate of coke formation, a TGA analysis of the reduced Ni-UGS catalyst (after reduction pre-treatment and before GSR reaction) (Fig. 8) indicated

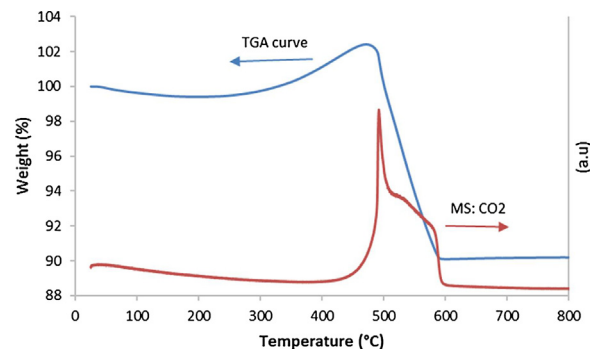


Fig. 7. TGA-MS of used Ni-UGS catalyst (after 48 h on GSR) in air atmosphere.

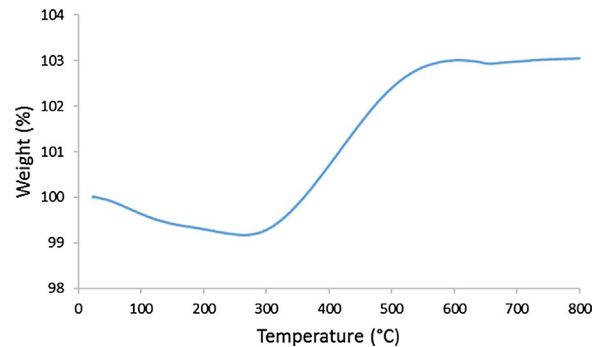


Fig. 8. TGA of reduced Ni-UGS catalyst in air atmosphere.

that about 3.8% mass gain (Table 4) can be attributed to the oxidation of reduced species in the temperature range of 270–600 °C. Comparing the amount of mass gain in the case of reduced Ni-UGS (3.8%) with that of used Ni-UGS (2.6%), one can estimate that actual mass loss due to CO₂ emission is nearly 1.2% higher than the value detected in TGA of used Ni-UGS in the range of 440–600 °C (12%). Accordingly, considering a weight loss of 13.2% due to gasification of carbonaceous deposits and 48 h as time on stream, the average rate of coke formation on the Ni-UGS catalyst under tested GSR conditions is estimated to be as low as $2.7 \text{ mg}_{\text{coke}} \text{ g}_{\text{cat}}^{-1} \text{ h}^{-1}$.

Generally, encapsulating, filamentous (whiskers), and pyrolytic type carbon are the most common types of carbon deposition that can be formed during steam reforming of hydrocarbons on Ni catalysts [62]. Diffusion and subsequent nucleation of adsorbed carbon atoms through Ni crystal lead to the formation of filamentous carbon (typically at $T > 450^\circ\text{C}$) with Ni-crystal atop [62]. In such condition, Ni surface is still active and only part of nickel particles can be deactivated as a result of blockage by the growing of carbon filaments in the pores of catalyst [63]. If accumulation of adsorbed carbon atoms on the free Ni surface increases, filament growth is suppressed and the Ni particles can be entrapped within a carbon layer; however, entrapment of a metal particle can be inhibited provided sufficient superstoichiometric excess of steam. Hence, in comparison with encapsulating and pyrolytic types, car-

Table 4
Measurement of weight changes during TGA in air.

Sample	Temperature Range (°C)	Weight Change (wt.%)	Cause of weight change
Reduced Ni-UGS ^a	25–270	-0.8	Loss of water
	270–600	+3.8	Oxidation of reduced species
Used Ni-UGS ^b	25–200	-0.6	Loss of water
	200–440	+2.6	Oxidation of reduced species
	440–600	-12	Simultaneous oxidation of reduced species and carbonaceous deposits

^a after pre-reduction step (before GSR reaction).

^b after pre-reduction step and 48 h on GSR reaction.

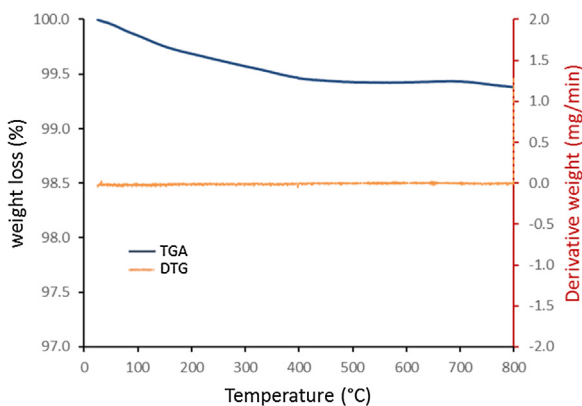


Fig. 9. TG/DTG curve for regenerated Ni-UGS catalyst.

bon filamentous would not necessarily result in a loss of catalyst activity [62–64]. As has been confirmed by several authors, the presence of basic MgO in catalyst formulation can limit dehydration and polymerization reactions which lead to the formation of encapsulating type carbon and quick catalyst deactivation [19,65]. The enhanced steam adsorption in presence of basic material can also help the oxidation of carbonaceous deposits [66]. Considering the discussion above (§3.4), it can be concluded that the different magnesium oxide species (such as MgO, MgFe₂O₄, (Ni,Mg)O and (MgO)(FeO) solid solutions) present in the Ni-UGS catalyst can assist coke gasification by promoting steam activation. Sufficient excess of H₂O/glycerol (S/C = 3) ratio used in our tests can also help oxidative removal of carbonaceous deposits. Moreover, the formation of (Ni,Mg)O solid solution can stabilize nickel and prevent catalyst sintering [67]. Wang and Lu [68] reported a long-term stability and limited carbon formation by using Ni/MgO as catalyst for CO₂ reforming of methane, which was attributed to a low sintering of nickel particles. These can justify the low rate of coke formation as estimated above and the stability of the Ni-UGS catalyst in the 48 h GSR experiment.

3.6. Regeneration of used Ni-UGS catalyst

An oxidative treatment was considered to investigate coke removal and possible recovery of pristine catalyst crystal structure. The used Ni-UGS catalyst was heated from room temperature up to 600 °C with a rate of 10 °C/min under air flow (40 STD mL min⁻¹) and maintained at 600 °C for 4 h. The conditions were selected based on the results of TG-MS analysis of used Ni-UGS in air atmosphere (Fig. 7), where CO₂ released by the burning of carbonaceous deposits terminates at 600 °C.

Fig. 9 shows the result of TG analysis of the regenerated Ni-UGS catalyst, carried out from ambient to 800 °C under air flow. Almost no loss of weight (less than 0.7%) was detected in the TG/DTG curve, confirming a total carbon removal. The XRD analysis of the catalyst after regeneration (Fig. 5d) also shows no peak related to graphitic type carbon. Moreover, a comparison with the XRD results for the fresh Ni-UGS catalyst (Fig. 5a) shows a complete recovery of the initial crystalline phases upon oxidizing of Ni-UGS in air atmosphere at 600 °C. According to Table 2, comparison of the BET surface area of regenerated Ni-UGS catalyst (7.9 m² g⁻¹) with those of used (59.5 m² g⁻¹) and fresh (10.3 m² g⁻¹) ones reveals that the surface area practically retrieved its initial value due the removal of filamentous carbon with high surface area.

Finally, the catalyst performance after regeneration was also evaluated. Fig. 10 shows the results of repeating GSR test for 4 h using the regenerated catalyst after 48 h on stream. Comparing with the results of fresh Ni-UGS, it can be seen that similar levels

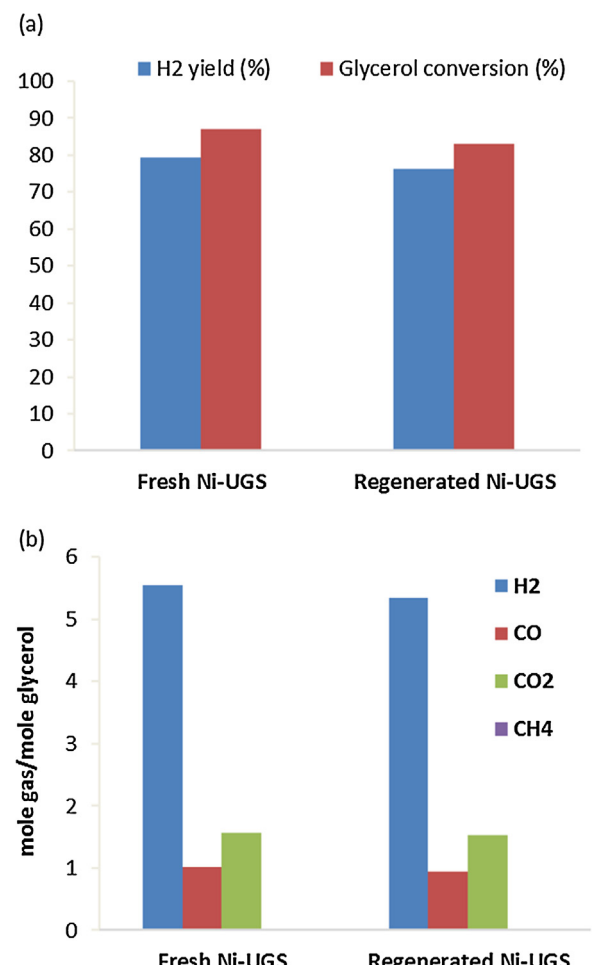


Fig. 10. Catalytic performances of fresh and regenerated Ni-UGS catalyst: (a) glycerol conversion to gaseous products and hydrogen yield; (b) gas products distribution.

of performance can be achieved by using the regenerated Ni-UGS catalyst.

4. Conclusion

A Ni-based catalyst (11.7 wt.%) was prepared by Ni incorporation into Fe/Mg containing UGS oxides metallurgical waste and investigated in steam reforming of glycerol. In comparison with the Ni-based commercial steam reforming catalyst (29.8 wt.% Ni), superior results were obtained in terms of glycerol conversion to gaseous products, H₂ yield, and H₂/CO molar ratio. Furthermore, the Ni-UGS catalyst showed a stable performance during 48 h on stream, where only slight structural changes with low average rate of filamentous type coke formation (approximately 2.7 mg_{coke} g_{cat}⁻¹ h⁻¹) were detected on the used catalyst. A complete coke removal as well as the recovery of pristine crystalline phases were achieved by oxidative treatment of used catalyst in air atmosphere.

These promising results were attributed to the synergy between (i) the ability of Ni for activation of C–H, C–C and O–H bonds of glycerol, (ii) the good dispersion and stabilization of Ni particles through formation of (Ni,Mg)O solid solution, (iii) the potential of basic MgO, which is in close contact with Ni in the form of (Ni,Mg)O solid solution, to activate hydroxyl species of glycerol, (iv) the ability of different magnesium and iron oxide species (such as MgO, Fe₃O₄, MgFe₂O₄ and (MgO)(FeO) solid solution) existed in the Ni-UGS catalyst under selected GSR operating conditions, to activate

steam and promote water gas shift reaction, and (v) the sufficient excess amount of water ($S/C = 3$) used in GSR experiments.

In conclusion, the results of this work clearly proved the capability of the Ni-UGS of acting as a powerful catalyst for GSR. A thorough parametric study and process optimisation will be the object of a forthcoming publication, to confirm the potential of this technology for industrial applications.

Acknowledgements

Financial support from the Fonds de recherche du Québec – Nature et technologies (FRQNT) and the Natural Sciences and Engineering Research Council of Canada (NSERC) are gratefully acknowledged.

References

- [1] S. Sharma, S.K. Ghoshal, Hydrogen the future transportation fuel: from production to applications, *Renewable Sustainable Energy Rev.* 43 (2015) 1151–1158.
- [2] C.A. Schwengber, H.J. Alves, R.A. Schaffner, F.A. da Silva, R. Sequinel, V.R. Bach, R.J. Ferracini, Overview of glycerol reforming for hydrogen production, *Renewable Sustainable Energy Rev.* 58 (2016) 259–266.
- [3] C.D. Dave, K.K. Pant, Renewable hydrogen generation by steam reforming of glycerol over zirconia promoted ceria supported catalyst, *Renewable Energy* 36 (2011) 3195–3202.
- [4] R.L. Manfro, N.F.P. Ribeiro, M.M.V.M. Souza, Production of hydrogen from steam reforming of glycerol using nickel catalysts supported on Al_2O_3 , CeO_2 and ZrO_2 , *Catal. Sustainable Energy* 1 (2013) 60–70.
- [5] B. Dou, Y. Song, C. Wang, H. Chen, Y. Xu, Hydrogen production from catalytic steam reforming of biodiesel byproduct glycerol: issues and challenges, *Renewable Sustainable Energy Rev.* 30 (2014) 950–960.
- [6] J.R.M. Almeida, L.C.L. Fávaro, B.F. Quirino, Biodiesel biorefinery: opportunities and challenges for microbial production of fuels and chemicals from glycerol waste, *Biotechnol. Biofuels* 48 (2012) 1–16.
- [7] J.M. Silva, M.A. Soria, L.M. Madeira, Challenges and strategies for optimization of glycerol steam reforming process, *Renewable Sustainable Energy Rev.* 42 (2015) 1187–1213.
- [8] Y.-C. Lin, Catalytic valorization of glycerol to hydrogen and syngas, *Int. J. Hydrogen Energy* 38 (2013) 2678–2700.
- [9] M. Gupta, N. Kumar, Scope and opportunities of using glycerol as an energy source, *Renewable Sustainable Energy Rev.* 16 (2012) 4551–4556.
- [10] M. Stelmachowski, Utilization of glycerol, a by-product of the transesterification process of vegetable oils: a review, *Ecol. Chem. Eng. S* 18 (2011) 9–30.
- [11] N.H. Tran, G.S. Kannangara, Conversion of glycerol to hydrogen rich gas, *Chem. Soc. Rev.* 42 (2013) 9454–9479.
- [12] G. Nahar, V. Dupont, Hydrogen via steam reforming of liquid biofeedstock, *Biofuels* 3 (2012) 167–191.
- [13] I. Iliuta, H.R. Radfarnia, M.C. Iliuta, Hydrogen production by sorption-enhanced steam glycerol reforming: sorption kinetics and reactor simulation, *AIChE J.* 59 (2013) 2105–2118.
- [14] I. Iliuta, M.C. Iliuta, Biosyngas production in an integrated aqueous-phase glycerol reforming/chemical looping combustion process, *Ind. Eng. Chem. Res.* 52 (2013) 16142–16161.
- [15] I. Rossetti, A. Gallo, V. Dal Santo, C.L. Bianchi, V. Nichele, M. Signoretto, E. Finocchio, G. Ramis, A. Di Michele, Nickel catalysts supported over TiO_2 , SiO_2 and ZrO_2 for the steam reforming of glycerol, *Chem. Cat. Chem.* 5 (2013) 294–306.
- [16] V. Nichele, M. Signoretto, F. Menegazzo, A. Gallo, V. Dal Santo, G. Cruciani, G. Cerrato, Glycerol steam reforming for hydrogen production: design of Ni supported catalysts, *Appl. Catal. B* 111–112 (2012) 225–232.
- [17] P.V. Mathure, S. Ganguly, A.V. Patwardhan, R.K. Saha, Steam reforming of ethanol using a commercial nickel-based catalyst, *Ind. Eng. Chem. Res.* 46 (2007) 8471–8479.
- [18] S. Li, J. Gong, Strategies for improving the performance and stability of Ni-based catalysts for reforming reactions, *Chem. Soc. Rev.* 43 (2014) 7245–7256.
- [19] L.F. Bobadilla, A. Penkova, F. Romero-Sarria, M.A. Centeno, J.A. Odriozola, Influence of the acid–base properties over $\text{NiSn}/\text{MgO}-\text{Al}_2\text{O}_3$ catalysts in the hydrogen production from glycerol steam reforming, *Int. J. Hydrogen Energy* 39 (2014) 5704–5712.
- [20] K.Y. Koo, H.-S. Roh, Y.T. Seo, D.J. Seo, W.L. Yoon, S.B. Park, Coke study on MgO -promoted $\text{Ni}/\text{Al}_2\text{O}_3$ catalyst in combined H_2O and CO_2 reforming of methane for gas to liquid (GTL) process, *Appl. Catal. A* 340 (2008) 183–190.
- [21] J.R. Rostrup-Nielsen, New aspects of syngas production and use, *Catal. Today* 63 (200) (2016) 159–164.
- [22] A. Iriondo, V.L. Barrio, J.F. Cambra, P.L. Arias, M.B. Güemez, R.M. Navarro, M.C. Sánchez-Sánchez, J.L.G. Fierro, Hydrogen production from glycerol over nickel catalysts supported on Al_2O_3 modified by Mg, Zr Ce or La, *Top. Catal.* 49 (2008) 46–58.
- [23] H. Provendier, C. Petita, Ásb C. Estourne, S. Libs, A. Kiennemann, Stabilisation of active nickel catalysts in partial oxidation of methane to synthesis gas by iron addition, *Appl. Catal. A* 180 (1999) 163–173.
- [24] C.A. Franchini, W. Aranzaez, A.M. Duarte de Farias, G. Pecchi, M.A. Fraga, Ce-substituted LaNiO_3 mixed oxides as catalyst precursors for glycerol steam reforming, *Appl. Catal. B* 147 (2014) 193–202.
- [25] M. Koike, D. Li, Y. Nakagawa, K. Tomishige, A highly active and coke-resistant steam reforming catalyst comprising uniform nickel–iron alloy nanoparticles, *Chem. Sus. Chem.* 5 (2012) 2312–2314.
- [26] K.O. Christensen, D. Chen, R. Lødeng, A. Holmen, Effect of supports and Ni crystal size on carbon formation and sintering during steam methane reforming, *Appl. Catal. A* 314 (2006) 9–22.
- [27] I.E. Achouri, N. Abatzoglou, C. Fauteux-Lefebvre, N. Braidy, Diesel steam reforming: comparison of two nickel aluminate catalysts prepared by wet-impregnation and co-precipitation, *Catal. Today* 207 (2013) 13–20.
- [28] Y.-H. Huang, S.-F. Wang, A.-P. Tsai, S. Kameoka, Catalysts prepared from copper–nickel ferrites for the steam reforming of methanol, *J. Power Sources* 281 (2015) 138–145.
- [29] R. Benrabaa, H. Boukhlof, A. Löfberg, A. Rubbens, R.-N. Vannier, E. Bordes-Richard, A. Barama, Nickel ferrite spinel as catalyst precursor in the dry reforming of methane: synthesis, characterization and catalytic properties, *J. Nat. Gas Chem.* 21 (2012) 595–604.
- [30] H. Muroyama, R. Nakase, T. Matsui, K. Eguchi, Ethanol steam reforming over Ni-based spinel oxide, *Int. J. Hydrogen Energy* 35 (2010) 1575–1581.
- [31] A. Sarvamini, F. Larachi, Catalytic oxygenless steam cracking of syngas-containing benzene model tar compound over natural Fe-bearing silicate minerals, *Fuel* 97 (2012) 741–750.
- [32] A. Sarvamini, F. Larachi, Mössbauer spectroscopy and catalytic reaction studies of Chrysotile-catalyzed steam reforming of Benzene, *J. Phys. Chem. C* 115 (2011) 6841–6848.
- [33] J.N. Kuhn, Z. Zhao, L.G. Felix, R.B. Slimane, C.W. Choi, U.S. Ozkan, Olivine catalysts for methane- and tar-steam reforming, *Appl. Catal. B* 81 (2008) 14–26.
- [34] J.N. Kuhn, Z. Zhao, A. Senefeld-Naber, L.G. Felix, R.B. Slimane, C.W. Choi, U.S. Ozkan, Ni-olivine catalysts prepared by thermal impregnation: structure, steam reforming activity, and stability, *Appl. Catal. A* 341 (2008) 43–49.
- [35] K. Takabane, K. Nagaoaka, K. Narai, K. Aika, Titania-supported cobalt and nickel bimetallic catalysts for carbon dioxide reforming of methane, *J. Catal.* 232 (2005) 268–275.
- [36] C. Courson, E. Makaga, C. Petit, A. Kiennemann, Development of Ni catalysts for gas production from biomass gasification. Reactivity in steam- and dry-reforming, *Catal. Today* 63 (2000) 427–437.
- [37] D. Świernyński, S. Libs, C. Courson, A. Kiennemann, Steam reforming of tar from a biomass gasification process over Ni/olivine catalyst using toluene as a model compound, *Appl. Catal. B* 74 (2007) 211–222.
- [38] D. Swierczynski, C. Courson, L. Bedel, A. Kiennemann, J. Guille, Characterization of Ni-Fe/MgO/Olivine catalyst for fluidized bed steam gasification of biomass, *Chem. Mater.* 18 (2006) 4025–4032.
- [39] M. Guéguin, F. Cardarelli, Chemistry and mineralogy of titania-rich slags. Part 1-Hemo-Ilmenite, sulphate, and upgraded titania slags, *Miner. Process. Extr. Metall. Rev.* 28 (2007) 1–58.
- [40] J. Ashok, S. Kawi, Nickel–iron alloy supported over iron–alumina catalysts for steam reforming of biomass tar model compound, *ACS Catal.* 4 (2014) 289–301.
- [41] L. Wang, D. Li, M. Koike, S. Koso, Y. Nakagawa, Y. Xu, K. Tomishige, Catalytic performance and characterization of Ni–Fe catalysts for the steam reforming of tar from biomass pyrolysis to synthesis gas, *Appl. Catal. A* 392 (2011) 248–255.
- [42] M. Chamoumi, N. Abatzoglou, J. Blanchard, M.C. Iliuta, F. Larachi, Dry reforming of methane with a new catalyst derived from a negative value mining residue spinellized with nickel, *Catal. Today* 291 (2017) 86–98.
- [43] J. Sun, L. Zhang, C. Ge, C. Tang, L. Dong, Comparative study on the catalytic CO oxidation properties of CuO/CeO_2 catalysts prepared by solid state and wet impregnation, *Chin. J. Catal.* 35 (2014) 1347–1358.
- [44] C. Tang, B. Sun, J. Sun, X. Hong, Y. Deng, F. Gao, L. Dong, Solid state preparation of NiO/CeO_2 catalyst for NO reduction, *Catal. Today* 281 (2017) 575–582.
- [45] Z. Zhang, Y. Liu, G. Yao, G. Zu, Y. Hao, Synthesis and characterization of NiFe_2O_4 nanoparticles via solid-state reaction, *Int. J. Appl. Ceram. Technol.* 10 (2013) 142–149.
- [46] T.K. Kundu, S. Mishra, Nanocrystalline spinel ferrites by solid state reaction route, *Bull. Mater. Sci.* 31 (2008) 507–510.
- [47] A.R. West, *Solid State Chemistry and Its Applications*, John Wiley & Sons, New York, 1984.
- [48] R.C. Turner, I. Hoffman, D. Chen, Thermogravimetry of the dehydration of $\text{Mg}(\text{OH})_2$, *Can. J. Chem.* 41 (1962) 243–252.
- [49] E. Bolshak, S. Abelló, D. Montané, Ethanol steam reforming over Ni–Fe-based hydrotalcites: effect of iron content and reaction temperature, *Int. J. Hydrogen Energy* 38 (2013) 5594–5604.
- [50] Z. Zhang, Y. Liu, G. Yao, G. Zu, X. Zhang, J. Ma, Solid-state reaction synthesis of NiFe_2O_4 nanoparticles by optimizing the synthetic conditions, *Physica E* 45 (2012) 122–129.
- [51] W.M. Keely, H.W. Maynor, Thermal studies of nickel, cobalt, iron, and copper oxides and nitrates, *J. Chem. Eng. Data* 8 (1963) 231–297.
- [52] M. Zangouei, A.Z. Moghaddam, M. Arasteh, The influence of nickel loading on reducibility of $\text{NiO}/\text{Al}_2\text{O}_3$ catalysts synthesized by sol-gel method, *Chem. Eng. Res. Bull.* 14 (2010).

[53] H. Jens, Industrial Catalysis, John Wiley & Sons, Germany, 2006.

[54] H. Chen, Y. Ding, N.T. Cong, B. Dou, V. Dupont, M. Ghadiri, P.T. Williams, A comparative study on hydrogen production from steam-glycerol reforming: thermodynamics and experimental, *Renewable Energy* 36 (2011) 779–788.

[55] H. Toshihide, I. Na-oki, M. Takanori, S. Toshimitsu, Production of hydrogen by steam reforming of glycerin on ruthenium catalyst, *Energy Fuels* 19 (2005) 1761–1762.

[56] D.G. Rethwisch, J.A. Dumesic, The effect of metal-oxygen bond strength on properties of oxides: II. Water gas shift over bulk oxides, *Appl. Catal.* 21 (1986) 97–109.

[57] A. Boudjemaa, C. Daniel, C. Mirodatos, M. Trari, A. Auoux, R. Bouarab, In situ DRIFTS studies of high-temperature water-gas shift reaction on chromium-free iron oxide catalysts, *C. R. Chim.* 14 (2011) 534–538.

[58] D.-W. Lee, M.S. Lee, J.Y. Lee, S. Kim, H.-J. Eom, D.J. Moon, K.-Y. Lee, The review of Cr-free Fe-based catalysts for high-temperature water-gas shift reactions, *Catal. Today* 210 (2013) 2–9.

[59] R. Benraabaa, A. Löfberg, J. Guerrero Caballero, E. Bordes-Richard, A. Rubbens, R.-N. Vannier, H. Boukhlouf, A. Barama, Sol-gel synthesis and characterization of silica supported nickel ferrite catalysts for dry reforming of methane, *Catal. Commun.* 58 (2015) 127–131.

[60] R. Benraabaa, A. Löfberg, A. Rubbens, E. Bordes-Richard, R.N. Vannier, A. Barama, Structure, reactivity and catalytic properties of nanoparticles of nickel ferrite in the dry reforming of methane, *Catal. Today* 203 (2013) 188–195.

[61] K. Watanabe, T. Miyao, K. Higashiyama, H. Yamashita, M. Watanabe, Preparation of a mesoporous ceria-zirconia supported Ni-Fe catalyst for the high temperature water-gas shift reaction, *Catal. Commun.* 12 (2011) 976–979.

[62] J.R. Rostrup-Nielsen, Catalytic steam reforming, in: J.R. Anderson, M. Boudart (Eds.), *Catalysis Science and Technology*, Springer, 1984.

[63] S. Abelló, E. Bolshak, D. Montané, Ni-Fe catalysts derived from hydrotalcite-like precursors for hydrogen production by ethanol steam reforming, *Appl. Catal. A* 450 (2013) 261–274.

[64] C.H. Bartholomew, Carbon deposition in steam reforming and methanation, *Catal. Rev. Sci. Eng.* 24 (2007) 67–112.

[65] S. Freni, S. Cavallaro, N. Mondello, L. Spadaro, F. Frusteri, Production of hydrogen for MC fuel cell by steam reforming of ethanol over MgO supported Ni and Co catalysts, *Catal. Commun.* 4 (2003) 259–268.

[66] A.C. Basagiannis, X.E. Verykios, Steam reforming of the aqueous fraction of bio-oil over structured Ru/MgO/Al₂O₃ catalysts, *Catal. Today* 127 (2007) 256–264.

[67] V.R. Choudhary, B.S. Uphade, A.S. Mamman, Oxidative conversion of methane to syngas over Nickel supported on commercial low surface area porous catalyst carriers precoated with alkaline and rare earth oxides, *J. Catal.* 172 (1997) 281–293.

[68] S. Wang, G.Q.M. Lu, CO₂ reforming of methane on Ni catalysts: effects of the support phase and preparation technique, *Appl. Catal. B* 16 (1998) 269–277.